Available online at www.sciencedirect.com
SCIENCE DIRECT®
Journal of Sound and Vibration 289 (2006) 908–937
JOURNAL OF SOUND AND VIBRATION
www.elsevier.com/locate/jsvi

Optimized electric networks for vibration damping of piezoactuated beams

P. Bisegna[a,*], G. Caruso[b], F. Maceri[a]

[a]*Department of Civil Engineering, University of Rome "Tor Vergata", 00133 Rome, Italy*
[b]*Institute of Technology for Constructions, CNR, 00137 Rome, Italy*

Received 24 March 2004; received in revised form 21 January 2005; accepted 28 February 2005
Available online 21 June 2005

Abstract

This paper studies the multimodal vibration damping of an elastic beam equipped with multiple piezoelectric actuators connected to an electric network. Two analytical models of the electromechanical coupled structure are considered: a homogenized one, accurate when a large number of actuators is employed, is used to derive simple design criteria for the electric network; and a discrete one, able to face real situations when few actuators are employed, is adopted to test the network performance, defined as the exponential time-decay rate of the free vibrations of the controlled structure. Some electric networks are presented and compared in simulation to networks previously proposed in the literature, in order to evaluate their performances in broadband vibration control.

1. Introduction

Piezoelectric sensors and actuators are widely used for vibration control, e.g., in aeronautic structures and precision manipulators, due to their lightness and easy integrability to the host structure [1].

Piezoelectric devices can be employed in active and hybrid vibration control schemes [2,3], requiring to design proper compensators and signal amplifiers to drive the actuators. Passive

*Corresponding author. Tel.: +39 06 72597097; fax: +39 06 72597005.
E-mail address: bisegna@uniroma2.it (P. Bisegna).

0022-460X/$ - see front matter © 2005 Elsevier Ltd. All rights reserved.
doi:10.1016/j.jsv.2005.02.045

vibration control is a simpler and cheaper technique, which is inherently stable and robust. It is implemented by shunting the piezoelectric devices on suitable electric circuits able to dissipate electric energy into heat through resistive components [4].

The most popular example of passive control scheme employs a single piezoelectric actuator and a resistive–inductive shunt (e.g., [4,5]). It is effective on one single structural eigenmode, since the shunt inductance can compensate the capacitive impedance of the piezoelectric actuator at the tuning frequency only.

Multimodal passive vibration damping is a more difficult task. Some significant results in this direction can be found in the literature. In Refs. [6,7] a single piezoelectric actuator is shunted to an electric network composed by parallel resistive–inductive–capacitive branches, each one tuned on a structural eigenmode. A similar approach is adopted in [8], where the capacitors of the parallel branches are replaced by current blockings, each one composed by the parallel of a capacitor and an inductor.

A multimodal damping system can be obtained also by means of a circuit containing a negative capacitance [9], used to compensate the inherent capacitive impedance of the piezoelectric actuator over a large frequency band [10–12]. However, this control system is not a passive one, since the implementation of a negative capacitance requires the use of active components.

A different strategy for multimodal damping [13–15] has been receiving much attention by researchers, and seems to be very promising also in applications to some related fields such as vibration delocalization in periodic structures [16] and localization of wave propagation in rods [17]. This strategy is based on the use of several piezoelectric actuators, bonded on a vibrating structure and connected to each other and/or to the ground through an electric network. The interlink between multiple piezoelectric actuators, periodically placed on the controlled structure, can provide control actions able to attenuate structural vibrations on a large frequency band. The performance of this control system crucially depends on the choice of the electric components contained in the network and on their clever disposition. In Ref. [13] a rotationally periodic structure has been considered, composed by several identical substructures, each equipped with a piezoelectric actuator connected to a resistive–inductive shunt in series to an active controller. Exploiting the periodicity of the structure, uncoupled differential equations relevant to each spatial harmonic are obtained, and an effective damping of all the spatial harmonics is achieved by properly choosing the active control law. The passive control schemes proposed in Refs. [14,15] act on a beam equipped with equally-spaced piezoelectric actuators connected to periodic electric networks containing resistive–inductive components. A continuous homogenized model of the electromechanical vibrating structure is employed. Uncoupled equations for each eigenmode are obtained and used for the optimization of the electric components. The optimal values turn out to depend on the eigenmode, so that those schemes are effective on a limited frequency band. Moreover, the homogenization approach is accurate when a large number of actuators is adopted: hence, it would be useful to test networks designed on the basis of a continuous model against the real discrete distribution of the actuators, often limited to few units for technological reasons.

This paper deals with vibration control of beams equipped with multiple piezoelectric actuators. It is aimed to develop control schemes which are effective on several eigenmodes and employ simple electric networks. The performance of each network is evaluated on the basis of the impulsive response of the controlled structure. More precisely, the performance index is defined as the exponential time-decay rate (ETDR) of the free vibrations, which is the maximum of the real

part of the system poles. Accordingly, the optimization process of each network relies on the pole placement technique, previously employed in the case of a single actuator [4,5].

As design tools, different models of the controlled structure are presented. A semi-continuous model, based on a continuous Euler–Bernoulli model for the beam and taking into account the actual discrete disposition of the actuators, is first presented. Two simplified models, more easily handled in applications, are then derived. A fully continuous model is obtained by using homogenization techniques; it yields simple design criteria for the electric networks. Furthermore, a fully discrete model is derived by means of standard approximation techniques; it is suitable to describe the real discrete distribution of the actuators and is used to evaluate the performance of each considered electric network.

As a case study, a simply-supported beam equipped with multiple equally-spaced piezoelectric actuators is considered. This analysis allows closed-form computations, and inspires the design of electric networks for different boundary conditions [18].

Several electric networks previously presented in the literature are analyzed and new ones are here proposed and evaluated.

The paper is organized as follows. The semi-continuous model of the electromechanical vibrating beam is presented in Section 2. The fully discrete model is derived in Section 3. A gallery of networks is presented in Section 4, classified into periodic (Section 4.1) and nonperiodic (Section 4.2). In the case of periodic networks, an homogenization limit is computed, leading to the fully continuous model presented in Section 5. The optimization criterium is discussed in Section 6. In Section 7 the case-study problem of a simply-supported beam equipped with equally-spaced actuators is considered. A closed form solution for this problem is derived according to both the continuous homogenized model (Section 7.1) and to the fully discrete model (Section 7.2). The solution in the case of the discrete model involves some lengthy calculations, reported in Appendix A. The performance evaluation of the proposed electric networks is presented in Section 8. In particular, a case-study structure is presented in Section 8.1, dimensionless parameters are introduced in Section 8.2, the periodic networks are analyzed in Section 8.3, and the nonperiodic networks in Section 8.4. In the case of periodic networks, the optimization is performed first according to the continuous homogenized model (Sections 8.3.2 and 8.3.3) and then by using the more accurate discrete model (Section 8.3.4), in order to highlight the difference in accuracy between the two models.

2. Semi-continuous model

In this section a dynamical model describing the behavior of a beam equipped with several piezoelectric actuators connected by an electric network is presented. This model is semi-continuous, since it arranges a continuous model for the beam and a discrete model for the actuators and the electric network.

The beam has length l and has a rectangular cross section, with thickness h, width b and flexural moment of inertia $J = bh^3/12$. It is comprised by a linearly elastic isotropic material with Young modulus E and Poisson ratio ν. The mass density per unit length is denoted by ρ. A Cartesian frame (O, x, y, z) is introduced, with $z \in (0, l)$ spanning the beam length. According to this notation, (y, z) is the flexure plane of the beam.

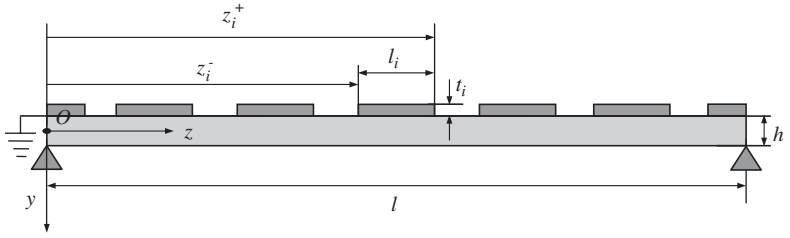

Fig. 1. Piezoactuated beam.

The beam is actuated by N_p piezoelectric devices bonded on its surface (Fig. 1). The ith actuator is supported on the interval (z_i^-, z_i^+), whose characteristic function is $\chi_i(z)$; the actuator length is $l_i = z_i^+ - z_i^-$; its width is b_i and its thickness is t_i, which is small compared to the in-plane dimensions l_i, b_i and to the beam thickness h. The actuators are comprised by a transversely isotropic, linearly piezoelectric material with transverse-isotropy axis oriented in the thickness direction. According to the Voigt notation, the relevant constitutive relationship is described by the five closed-circuit elastic constants c_{11}, c_{12}, c_{13}, c_{33} and c_{44}, the two clamped permittivity constants ε_{11} and ε_{33}, and the three piezoelectric constants e_{31}, e_{33} and e_{15} [19].

The displacement field in the beam is represented according to the Euler–Bernoulli model, and the beam deflection at the time t is denoted by $v(z, t)$. For the sake of simplicity, the actuators are assumed to contribute negligibly to the bending stiffness of the structure. The opposite surfaces of each actuator are covered by electrodes. The electrode bonded to the beam is grounded; the opposite one has an electric potential denoted by φ_i and stores an electric charge denoted by q_i. The voltages φ_i and the charges q_i are arranged in vectors $\boldsymbol{\varphi}$ and $\mathbf{q}$, respectively, with N_p components.

The equilibrium equation of the beam and the charge balance equation of the piezoelectric actuators, written in the Laplace domain, are [20–22]:

$$EJv'''' = -\rho(s^2 v - \dot{v}_0 - s v_0) + \mathbf{k} \cdot \boldsymbol{\varphi}, \tag{1}$$

$$\mathbf{C}^p \boldsymbol{\varphi} + \int_0^l \mathbf{k} v \, \mathrm{d}z = \mathbf{q}. \tag{2}$$

Here differentiation with respect to z is denoted by a prime; scalar product is denoted by a dot; s is the Laplace variable and, with a slight abuse of notation, the Laplace transform of a function f is denoted again by f; $v_0(z)$ and $\dot{v}_0(z)$ are the initial displacement and velocity, respectively, and $s^2 v - \dot{v}_0 - s v_0$ is the Laplace transform of the second time derivative of the beam deflection; the matrix $\mathbf{C}^p$ is diagonal, and its ith entry $C^p_{ii} = \overline{\varepsilon}_{33} b_i l_i / t_i$ is the clamped electric capacity of the ith piezoelectric actuator; the vector $\mathbf{k}$, whose entries are

$$k_i = -\frac{h}{2} \overline{e}_{31} b_i \chi_i'' = \frac{h}{2} \overline{e}_{31} b_i [\delta'(z - z_i^+) - \delta'(z - z_i^-)] \tag{3}$$

takes into account the piezoelectric coupling. Here δ is the Dirac function, and the derivatives are intended in the sense of distributions. In particular, $k_i \varphi_i$ represents a pair of opposite couples of magnitude $\pm(h/2)\overline{e}_{31} b_i \varphi_i$ located at $z_i^{\pm}$, generated by the converse piezoelectric effect; on the

other hand,

$$\int_0^l k_i v \, \mathrm{d}z = \frac{h}{2} \overline{e}_{31} b_i [-v'(z_i^+) - (-v'(z_i^-))] \tag{4}$$

is the charge driven on the ith actuator by the beam deflection, due to the direct piezoelectric effect. The material constants $\overline{\varepsilon}_{33}$ and $\overline{e}_{31}$ entering the piezoelectric capacitances and coupling coefficients, respectively, are given by [20]

$$\overline{\varepsilon}_{33} = \varepsilon_{33} + e_{33}^2/c_{33}, \quad \overline{e}_{31} = e_{31} - c_{13}e_{33}/c_{33}. \tag{5}$$

In particular, the former is the reduced clamped permittivity in the transversal direction and the latter is the reduced piezoelectric coupling coefficient. They yield the charge density, respectively, induced by a transversal electric field or by an in-plane strain on a device under vanishing transversal normal stress.

The dynamical model of the coupled electromechanical system is completed by the following relationship between $\boldsymbol{\varphi}$ and $\mathbf{q}$:

$$s\mathbf{q} + \mathbf{A}(s)\boldsymbol{\varphi} = \mathbf{0}, \tag{6}$$

which depends upon the external electric network connecting the actuators to each other and to the ground. For the sake of simplicity, vanishing initial electric conditions are enforced. Hence, $s\mathbf{q}$ is the Laplace transform of the time derivative of the charge on the actuators. On the other hand, the electric admittance symmetric matrix $\mathbf{A}(s)$, whose dependence on s is here emphasized, contains on the main diagonal at position (i, i), the sum of all the electric admittances reaching the ith actuator, and off diagonal at position (i,j), $i \neq j$, the opposite of the electric admittance between the ith and jth actuator. As a consequence, $\mathbf{A}(s)\boldsymbol{\varphi}$ is the current from the actuators to the network or to the ground. Hence, Eq. (6) expresses a current balance; in Section 4 it will be specialized to several different electric networks.

The electric charge $\mathbf{q}$ can be substituted from Eq. (6) into Eq. (2), leading to

$$\int_0^l \mathbf{k} v \, \mathrm{d}z + \left[\mathbf{C}^p + \frac{1}{s}\mathbf{A}(s)\right]\boldsymbol{\varphi} = \mathbf{0}. \tag{7}$$

Eqs. (1) and (7) constitute the semi-continuous model of the piezoactuated beam, which can be recast in the following variational formulation:

$$\operatorname*{stat}_{v,\boldsymbol{\varphi}} \left\{ \int_0^l \left[\frac{EJ}{2}(v'')^2 + \frac{\rho s^2}{2} v^2 - \rho(\dot{v}_0 + s v_0) v - \mathbf{k} \cdot \boldsymbol{\varphi} \, v \right] \mathrm{d}z - \frac{1}{2}\boldsymbol{\varphi} \cdot \left[\mathbf{C}^p + \frac{1}{s}\mathbf{A}(s)\right]\boldsymbol{\varphi} \right\}. \tag{8}$$

This formulation straightforwardly yields the compatible boundary conditions and can take into account nonhomogeneous variational boundary data by adding suitable linear terms to the involved functional [23]. It constitutes the basis of the discrete model presented in Section 3.

3. Discrete model: modal analysis

A completely discrete model of the piezoactuated beam can be obtained by discretizing the function v involved in the variational formulation (8) of the semi-continuous model. To this end,

the function v is approximated as follows:

$$v(z,s)=\sum_{j=1}^{n} v_j(s) f_j(z), \tag{9}$$

where $f_j(z)$ are fixed shape functions satisfying the essential boundary conditions, $v_j(s)$ are the mechanical unknowns (e.g., nodal values or Ritz–Raleigh coefficients), arranged into a vector $\mathbf{v}$ and n is the number of mechanical degrees of freedom of the discretized model (e.g., [21]). This leads to the equations:

$$\mathbf{M}\left(s^2\mathbf{v}-\dot{\mathbf{v}}_0-s\mathbf{v}_0\right)+\mathbf{K}_{mm}\mathbf{v}+\mathbf{K}_{me}\boldsymbol{\varphi}=\mathbf{0}, \tag{10}$$

$$\mathbf{K}_{me}^{\mathrm{T}}\mathbf{v}-\left[\mathbf{C}^p+\frac{1}{s}\mathbf{A}(s)\right]\boldsymbol{\varphi}=\mathbf{0}. \tag{11}$$

Here $\mathbf{M}$ is the mass matrix, $\mathbf{K}_{mm}$ is the stiffness matrix, $\mathbf{K}_{me}$ is the piezoelectric coupling matrix and a superscript T denotes transposition; it is here remarked that all these matrices are real. In the Laplace domain, Eq. (10) expresses the discrete mechanical equilibrium between the inertial term $-\mathbf{M}(s^2\mathbf{v}-\dot{\mathbf{v}}_0-s\mathbf{v}_0)$, the elastic term $-\mathbf{K}_{mm}\mathbf{v}$ and the piezoelectric term $-\mathbf{K}_{me}\boldsymbol{\varphi}$ due to the actuators. In the Laplace domain, Eq. (11) stipulates that the electric charge stored by the actuators, which is composed by the capacitive term $\mathbf{C}^p\boldsymbol{\varphi}$ and piezoelectric term $-\mathbf{K}_{me}^{\mathrm{T}}\mathbf{v}$, is just the charge $-(1/s)\mathbf{A}(s)\boldsymbol{\varphi}$ flowed from the network or the ground to the actuators.

In order to obtain a simpler form of Eq. (10), a modal analysis is performed. Consequently, the change of variable $\mathbf{v}=\mathbf{V}\mathbf{y}$ is enforced, where the matrix $\mathbf{V}$ is determined by imposing that $\mathbf{V}^{\mathrm{T}}\mathbf{M}\mathbf{V}$ is the identity matrix and $\mathbf{V}^{\mathrm{T}}\mathbf{K}_{mm}\mathbf{V}=\boldsymbol{\Omega}^2$ is a positive-definite diagonal matrix. Accordingly, Eqs. (10) and (11) are transformed into:

$$s^2\mathbf{y}-\dot{\mathbf{y}}_0-s\mathbf{y}_0+\boldsymbol{\Omega}^2\mathbf{y}+\boldsymbol{\Lambda}\boldsymbol{\varphi}=\mathbf{0}, \tag{12}$$

$$\boldsymbol{\Lambda}^{\mathrm{T}}\mathbf{y}-\left[\mathbf{C}^p+\frac{1}{s}\mathbf{A}(s)\right]\boldsymbol{\varphi}=\mathbf{0}. \tag{13}$$

The diagonal components of $\boldsymbol{\Omega}$ are the modal circular frequencies at shorted actuators (i.e., when $\boldsymbol{\varphi}=\mathbf{0}$), and the columns of $\boldsymbol{\Lambda}=\mathbf{V}^{\mathrm{T}}\mathbf{K}_{me}$ contain the modal piezoelectric coupling coefficients relevant to each actuator. The columns of $\mathbf{V}$ are the modal structural eigenvectors at shorted actuators, and $\mathbf{y}$ is the vector of the modal coordinates. Moreover, $\mathbf{y}_0=\mathbf{V}^{-1}\mathbf{v}_0$ and $\dot{\mathbf{y}}_0=\mathbf{V}^{-1}\dot{\mathbf{v}}_0$.

A modal reduction could be performed by retaining only the most significant components of $\mathbf{y}$ and the corresponding equilibrium equations in Eq. (12).

It is emphasized that the modal mechanical unknowns $\mathbf{y}$ are coupled to each other by the electric unknowns $\boldsymbol{\varphi}$, since the matrices $\boldsymbol{\Lambda}$ and $\mathbf{A}(s)$ are not, in general, diagonal. However, they can be transformed into diagonal in special cases, as it will be shown in Section 7.2.

4. Electric networks

In this section some electric networks are analyzed. Networks composed by a periodic arrangement of admittances are considered in Section 4.1. They allow an homogenization process,

which will be performed in Section 5. Networks which do not share any periodicity property are considered in Section 4.2.

4.1. Periodic electric networks

This kind of electric networks is composed by a periodic arrangement of admittances.

In Fig. 2 the admittance $A_0(s)$ connects each actuator to the ground. The current balance relevant to the typical actuator i is

$$sq_i + A_0(s)\varphi_i = 0. \tag{14}$$

In Fig. 3 the admittance $A_2(s)$ connects each actuator to the adjacent ones. The current balance relevant to the typical actuator i is

$$sq_i + A_2(s)(-\varphi_{i+1} + 2\varphi_i - \varphi_{i-1}) = 0. \tag{15}$$

In Fig. 4 the admittance $4A_4(s)$ connects the typical actuator i to the actuators $i-1$ and $i+1$, and the admittance $-A_4(s)$ connects the actuator i to the actuators $i-2$ and $i+2$. The current balance

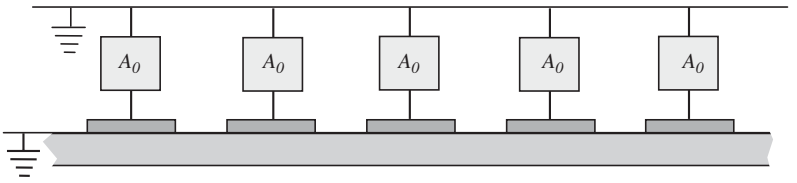

Fig. 2. Zeroth-order periodic electric network PN0.

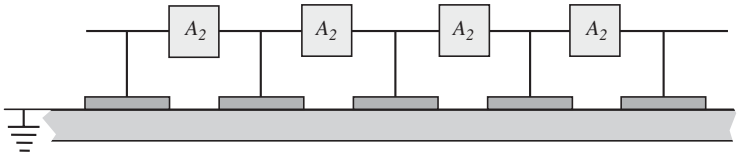

Fig. 3. Second-order periodic electric network PN2.

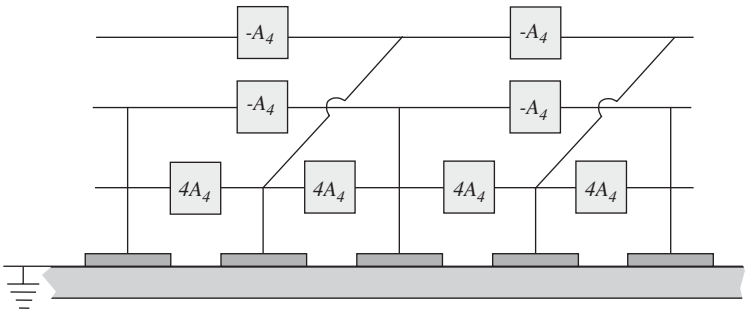

Fig. 4. Fourth-order periodic electric network PN4.

relevant to the typical ith piezoelectric actuator reads as follows [15]:

$$sq_i + A_4(s)(\varphi_{i+2} - 4\varphi_{i+1} + 6\varphi_i - 4\varphi_{i-1} + \varphi_{i-2}) = 0. \tag{16}$$

It is pointed out that the network in Fig. 4 involves both the admittances $4A_4(s)$ and $-A_4(s)$, so that it is not a truly passive network.

Here $A_0(s)$, $A_2(s)$ and $A_4(s)$ are, respectively, referred to as zeroth-, second- and fourth-order line admittance. In fact, in Section 5 it will be proved that, in the homogenization limit, under suitable scaling conditions, Eqs. (14), (15) and (16), respectively, originate terms involving the potential φ, its second-order spatial derivative φ'', and its fourth-order spatial derivative φ''''. Accordingly, the electric networks in Figs. 2, 3 and 4 are, respectively, referred to as zeroth-, second- and fourth-order periodic network and are denoted by the acronyms PN0, PN2, PN4. Of course, higher-order electric networks could in principle be considered, but the previous ones suffice for the purpose of vibration damping.

The periodic networks considered in the following are built up as the parallel of PN0, PN2 and PN4. Accordingly, the current balance relevant to the typical ith piezoelectric actuator reads in the general case as follows:

$$sq_i + A_0(s)\varphi_i + A_2(s)(-\varphi_{i+1} + 2\varphi_i - \varphi_{i-1}) + A_4(s)(\varphi_{i+2} - 4\varphi_{i+1} + 6\varphi_i - 4\varphi_{i-1} + \varphi_{i-2}) = 0. \tag{17}$$

4.2. Nonperiodic electric networks

The electric network sketched in Fig. 5 is obtained by shunting the typical actuator i on a suitable admittance $A^i(s)$, which, in general, is different for different actuators. On the basis of the analogy to the network PN0, it will be denoted by the acronym NPN0 (nonperiodic zeroth-order network). The current balance relevant to the actuator i is

$$sq_i + A^i(s)\varphi_i = 0. \tag{18}$$

The electric network sketched in Fig. 6 is obtained by connecting the typical actuator i with the adjacent actuators $i-1$ and $i+1$ by means of admittances $A^{i-1,i}(s)$ and $A^{i,i+1}(s)$, respectively.

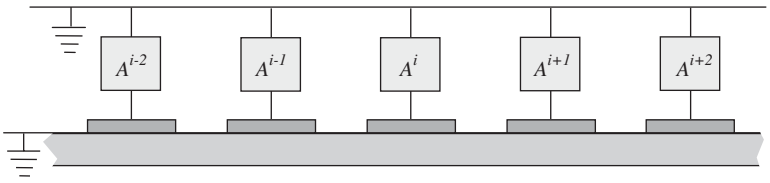

Fig. 5. Zeroth-order nonperiodic electric network NPN0.

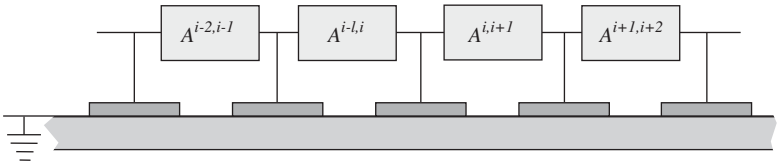

Fig. 6. Second-order nonperiodic electric network NPN2.

On the basis of the analogy with the network PN2, it will be denoted by the acronym NPN2 (nonperiodic second-order network). The current balance relevant to the actuator i is

$$sq_i + A^{i-1,i}(s)(\varphi_i - \varphi_{i-1}) + A^{i,i+1}(s)(\varphi_i - \varphi_{i+1}) = 0. \tag{19}$$

5. Continuous model: homogenization of periodic electric networks

The electric networks introduced in Section 4.1 are periodic in space. If the spatial period ε is small compared to the beam length l, one may be tempted to replace the discrete real distribution of the actuators by an equivalent continuous one, i.e., to perform an homogenization limit [24].

It is assumed that the actuators have the same length $l_i = \eta\varepsilon$, the same width $b_i = b$ and the same thickness $t_i = t$. Here η is the piezoelectric covering factor, i.e., the fraction of the spatial period (and hence, the fraction of the beam length) covered by the actuators. Let $D_\varepsilon = \bigcup_{i=1}^{N_p}(z_i^-, z_i^+)$ be the domain occupied by the actuators.

When the number of actuators N_p becomes very large, the function $\sum_{i=1}^{N_p}\chi_i$ weakly converges to η as $\varepsilon \to 0$. Moreover, it is assumed that:

- the mechanical displacement v strongly converges, together with its derivatives, to a limiting function which is again denoted by v;
- the piecewise constant electric potential $\sum_{i=1}^{N_p}\chi_i\varphi_i$, regarded as a function defined over D_ε, can be extended over $(0,l)$ uniformly with respect to ε to a smooth function $\tilde{\varphi}_\varepsilon$, which strongly converges, together with its derivatives, to a limiting function φ;
- the piecewise constant charge density $\sum_{i=1}^{N_p}\chi_i q_i/l_i$, regarded as a function defined over D_ε, can be extended over $(0,l)$ uniformly with respect to ε to a smooth function $\tilde{\sigma}_\varepsilon$, which strongly converges to a limiting charge density σ.

Then, in particular,

$$\sum_{i=1}^{N_p}\chi_i\varphi_i = \sum_{i=1}^{N_p}\chi_i\tilde{\varphi}_\varepsilon \to \eta\varphi, \quad \sum_{i=1}^{N_p}\frac{\chi_i q_i}{l_i} = \sum_{i=1}^{N_p}\chi_i\tilde{\sigma}_\varepsilon \to \eta\sigma. \tag{20}$$

A rigorous functional framework can be derived by using techniques similar to Ref. [24].

A weak version of Eq. (1) is now derived, in order to obtain its homogenization limit. To this end, Eq. (1) is multiplied by a smooth test function ψ compactly supported on $(0,l)$, and integrated over $(0,l)$, yielding

$$\int_0^l EJv''\psi''\,\mathrm{d}z = \int_0^l -\rho(s^2v - \dot{v}_0 - sv_0)\psi\,\mathrm{d}z - \sum_{i=1}^{N_p}\frac{h}{2}\overline{e}_{31}b\varphi_i[\psi'(z_i^+) - \psi'(z_i^-)]. \tag{21}$$

This equation is transformed into

$$\int_0^l EJv''\psi''\,\mathrm{d}z = \int_0^l -\rho(s^2v - \dot{v}_0 - sv_0)\psi\,\mathrm{d}z - \int_0^l \frac{h}{2}\overline{e}_{31}b\psi''\sum_{i=1}^{N_p}\varphi_i\chi_i\,\mathrm{d}z, \tag{22}$$

which yields in the limit:

$$\int_0^l EJv''\psi''\,\mathrm{d}z = \int_0^l -\rho(s^2v - \dot{v}_0 - sv_0)\psi\,\mathrm{d}z - \int_0^l K\psi''\varphi\,\mathrm{d}z, \tag{23}$$

whose strong version is

$$EJv'''' = -\rho(s^2v - \dot{v}_0 - sv_0) - K\varphi''. \tag{24}$$

On the other hand, Eq. (2), after multiplying by χ_i/l_i and summing over i, gives

$$\sum_{i=1}^{N_p} \frac{\bar{\varepsilon}_{33}b}{t}\chi_i\varphi_i - \sum_{i=1}^{N_p} \frac{h}{2}\bar{e}_{31}b\chi_i\frac{v'(z_i^+) - v'(z_i^-)}{l_i} = \sum_{i=1}^{N_p}\frac{\chi_i q_i}{l_i}, \tag{25}$$

which yields in the limit:

$$\Gamma\varphi - Kv'' = \eta\sigma. \tag{26}$$

Here

$$K = \frac{\eta h\bar{e}_{31}b}{2}, \quad \Gamma = \frac{\eta\bar{\varepsilon}_{33}b}{t}. \tag{27}$$

It can be easily recognized that Γ is the capacity per unit length of the homogenized distribution of the actuators. Analogously, K is the homogenized structural piezoelectric coupling coefficient, i.e., the charge density induced by a unit curvature of the beam. It is emphasized that σ is the charge density on the actuators, whereas $\eta\sigma$ is the charge density per unit length of the homogenized beam: the former is greater than the latter when the actuators do not entirely cover the beam length.

It remains to take the limit of Eq. (6). In order to analyze a specific class of periodic networks, Eq. (17) is considered instead. It is multiplied by χ_i/l_i and summed over i. Moreover, it is assumed that the line admittances $A_0(s)$, $A_2(s)$, and $A_4(s)$ rescale as follows:

$$A_0(s) = \varepsilon\hat{A}_0(s), \quad A_2(s) = \varepsilon^{-1}\hat{A}_2(s), \quad A_4(s) = \varepsilon^{-3}\hat{A}_4(s), \tag{28}$$

where $\hat{A}_0(s)$, $\hat{A}_2(s)$ and $\hat{A}_4(s)$ do not depend on ε. In particular, $\hat{A}_0(s)$ is the admittance toward the ground per unit length; analogously, $\hat{A}_2^{-1}(s)$ is the line impedance per unit length. As a consequence of these scalings, Eq. (17), after multiplying by χ_i/l_i and summing over i, gives

$$\begin{aligned} s\sum_{i=1}^{N_p}\frac{\chi_i q_i}{l_i} + \frac{\hat{A}_0(s)}{\eta}\sum_{i=1}^{N_p}\varphi_i\chi_i - \frac{\hat{A}_2(s)}{\eta}\sum_{i=1}^{N_p}\frac{\varphi_{i+1} - 2\varphi_i + \varphi_{i-1}}{\varepsilon^2}\chi_i \\ + \frac{\hat{A}_4(s)}{\eta}\sum_{i=1}^{N_p}\frac{\varphi_{i+2} - 4\varphi_{i+1} + 6\varphi_i - 4\varphi_{i-1} + \varphi_{i-2}}{\varepsilon^4}\chi_i = 0 \end{aligned} \tag{29}$$

and yields in the limit:

$$s\eta\sigma + \hat{A}_0(s)\varphi - \hat{A}_2(s)\varphi'' + \hat{A}_4(s)\varphi'''' = 0. \tag{30}$$

The charge density σ can be substituted from Eq. (30) into Eq. (26), yielding

$$\frac{1}{s}[\hat{A}_0(s)\varphi - \hat{A}_2(s)\varphi'' + \hat{A}_4(s)\varphi''''] + \Gamma\varphi - Kv'' = 0. \tag{31}$$

Eqs. (24) and (31) constitute the continuous homogenized model of the piezoactuated beam. They can be recast in the following variational formulation:

$$\operatorname*{stat}_{v,\varphi} \int_0^l \left\{ \frac{1}{2} EJ(v'')^2 + K\varphi v'' + \frac{\rho s^2}{2} v^2 - \rho(\dot{v}_0 + s v_0)v \right. \\ \left. - \frac{\Gamma}{2}\varphi^2 - \frac{1}{2s}[\hat{A}_0(s)\varphi^2 + \hat{A}_2(s)(\varphi')^2 + \hat{A}_4(s)(\varphi'')^2] \right\} \mathrm{d}z. \tag{32}$$

This formulation immediately yields the compatible boundary conditions requested in order to complete the problem, to be imposed at the boundaries $z = 0$ and l:

$$v \text{ assigned} \quad \text{or} \quad EJv''' + K\varphi' = 0, \tag{33}$$

$$v' \text{ assigned} \quad \text{or} \quad EJv'' + K\varphi = 0, \tag{34}$$

$$\varphi \text{ assigned} \quad \text{or} \quad \frac{1}{s}(-\hat{A}_2(s)\varphi' + \hat{A}_4(s)\varphi''') = 0, \tag{35}$$

$$\varphi' \text{ assigned} \quad \text{or} \quad \frac{\hat{A}_4(s)}{s}\varphi'' = 0. \tag{36}$$

Of course, nonhomogeneous variational boundary data can be taken into account by adding suitable linear terms to functional (32) [23].

6. Optimization criterium

The continuous model (24), (31), to be completed by the boundary conditions (33)–(36), as well as the discrete model (12) and (13), involve admittances to be chosen in order to achieve an efficient vibration damping.

Designing the network admittances is an optimization problem which requires the choice of an objective function to be minimized. This choice reflects one's prejudices about vibration damping. Some authors introduce a sinusoidal forcing term in the model equations and choose an integral norm of the corresponding frequency response function as the objective function. That approach is suitable to study the forced response of the system.

In this paper the impulsive response of the controlled structure is considered. The objective function to be minimized is the ETDR of the free vibrations, which is defined as the maximum of the real part of the poles of the controlled system. Of course, the ETDR must be negative for the system to be stable. From a physical point of view, minimizing the ETDR amounts to making as fast as possible the time decay of the most-slowly exponentially-decaying term of the response.

7. Simply-supported beam with periodic electric networks

In this section, the case of the simply-supported beam, equipped with periodically spaced piezoelectric actuators connected to a periodic electric network, is thoroughly studied, by using both the continuous model and the discrete model. After a suitable choice of the electric boundary conditions, and by exploiting the periodicity property of the system, uncoupled dynamical

equations relevant to each structural eigenmode are obtained. Then, a closed-form analytical optimization of the electric components is performed such as to achieve a multimodal damping. The analysis of this case yields design criteria which turn out to be useful also for different boundary conditions [18] and different structural topologies, such as rotationally periodic structures [13].

7.1. Continuous model

The mechanical boundary conditions are given by Eqs. $(33)_1$ and $(34)_2$. It is convenient to choose as electric boundary conditions $(35)_1$ and $(36)_2$. Accordingly, it is easy to verify that the solution of Eqs. (24) and (31) can be written as follows:

$$v(z,s)=\sum_{j=1}^{+\infty}\sqrt{\frac{2}{\rho l}}v_j(s)\sin(\alpha_j z),\quad \varphi(z,s)=\sum_{j=1}^{+\infty}\sqrt{\frac{2}{l}}\varphi_j(s)\sin(\alpha_j z), \tag{37}$$

where $\alpha_j=\pi j/l$ and the coefficients $v_j(s)$ and $\varphi_j(s)$ satisfy the equation:

$$\begin{bmatrix} \dfrac{EJ}{\rho}\alpha_j^4+s^2 & -\dfrac{K\alpha_j^2}{\sqrt{\rho}} \\ -\dfrac{K\alpha_j^2}{\sqrt{\rho}} & -\Gamma-\dfrac{1}{s}[\hat{A}_0(s)+\alpha_j^2\hat{A}_2(s)+\alpha_j^4\hat{A}_4(s)] \end{bmatrix}\begin{bmatrix} v_j \\ \varphi_j \end{bmatrix}=\begin{bmatrix} \dot{v}_{0j}+sv_{0j} \\ 0 \end{bmatrix}, \tag{38}$$

where the initial displacement and velocity have been expanded according to Eq. $(37)_1$, with coefficients v_{0j} and $\dot{v}_{0j}$, respectively. It is pointed out that the modal components (v_j,φ_j) in Eq. (37), corresponding to a mode $j\in\mathbf{N}$, are uncoupled from the modal components $(v_{j'},\varphi_{j'})$, corresponding to another mode $j'\in\mathbf{N}$. The poles corresponding to the mode j are given by the values of s which make the determinant at the left-hand side of Eq. (38) vanish:

$$\left(\frac{EJ}{\rho}\alpha_j^4+s^2\right)\left\{\Gamma+\frac{1}{s}[\hat{A}_0(s)+\alpha_j^2\hat{A}_2(s)+\alpha_j^4\hat{A}_4(s)]\right\}+\frac{K^2\alpha_j^4}{\rho}=0. \tag{39}$$

All the poles of the system are obtained by collecting the roots of Eq. (39) over $j\in\mathbf{N}$.

As it was explained in Section 6, the optimization amounts to choosing the admittances $\hat{A}_0(s)$, $\hat{A}_2(s)$ and $\hat{A}_4(s)$ in order to minimize the maximum of the real part of the poles of the system. This is a difficult task, mainly due to the fact that the poles corresponding to all the modes must be considered at the same time. Indeed, one cannot perform the optimization by looking at one mode at a time, since the admittances, say $\hat{A}_0^{(j)}$, $\hat{A}_2^{(j)}$ and $\hat{A}_4^{(j)}$, which optimize the poles corresponding to a generic mode $j\in\mathbf{N}$ are in general different from the admittances, say $\hat{A}_0^{(j')}$, $\hat{A}_2^{(j')}$ and $\hat{A}_4^{(j')}$, which optimize the poles corresponding to another mode $j'\in\mathbf{N}$, due to the fact that j explicitly enters Eq. (39), through α_j. Thus, optimizing one mode at a time is inconclusive, since it would be unclear which set of admittances $\hat{A}_0^{(j)}$, $\hat{A}_2^{(j)}$ and $\hat{A}_4^{(j)}$ should be chosen.

However, a simple approach is proposed here, in order to overcome the difficulty of considering all the modes simultaneously. First, it is observed that when the piezoelectric actuators are shunted to the ground, i.e., when $\hat{A}_0$ tends to infinity, the poles of the system are

given by

$$\frac{EJ}{\rho}\alpha_j^4 + s^2 = 0, \quad \text{i.e., they are : } \left\{\pm \mathrm{I}\alpha_j^2\sqrt{\frac{EJ}{\rho}}\right\}_{j\in\mathbf{N}}, \tag{40}$$

where $\mathrm{I} = \sqrt{-1}$ is the imaginary unit. Analogously, when the piezoelectric actuators are not connected to each other or to the ground, i.e., when $\hat{A}_0 = \hat{A}_2 = \hat{A}_4 = 0$, the poles of the system are given by

$$\left(\frac{EJ}{\rho}\alpha_j^4 + s^2\right)\Gamma + \frac{K^2\alpha_j^4}{\rho} = 0, \quad \text{i.e., they are : } \left\{\pm \mathrm{I}\alpha_j^2\sqrt{\frac{EJ}{\rho} + \frac{K^2}{\rho\Gamma}}\right\}_{j\in\mathbf{N}}. \tag{41}$$

The poles in Eq. (40) (respectively, Eq. (41)) are purely imaginary, and correspond to the natural circular frequencies of the structure at shorted (respectively, open) actuators. These poles are proportional to α_j^2. This issue suggests to set

$$S_j = \frac{s}{\alpha_j^2}. \tag{42}$$

After this position, Eq. (39) is transformed into

$$\left(\frac{EJ}{\rho} + S_j^2\right)\left[\Gamma + \frac{1}{S_j}\left(\frac{\hat{A}_0(\alpha_j^2 S_j)}{\alpha_j^2} + \hat{A}_2(\alpha_j^2 S_j) + \alpha_j^2\hat{A}_4(\alpha_j^2 S_j)\right)\right] + \frac{K^2}{\rho} = 0. \tag{43}$$

It is emphasized that Eq. (43) turns out to be independent of α_j, provided that

$$\begin{aligned}
&\hat{A}_0 \text{ is a capacitive admittance, i.e., } \hat{A}_0(s) = s\hat{C},\\
&\hat{A}_2 \text{ is a Ohmic admittance, i.e., } \hat{A}_2(s) = 1/\hat{R},\\
&\hat{A}_4 \text{ is an inductive admittance, i.e., } \hat{A}_4(s) = 1/(s\hat{L}),
\end{aligned} \tag{44}$$

where $\hat{C}$, $\hat{R}$ and $\hat{L}$ are parameters to be optimally chosen. Indeed, when this is the case, Eq. (43) is transformed into

$$\left(\frac{EJ}{\rho} + S_j^2\right)\left[\Gamma + \frac{1}{S_j}\left(S_j\hat{C} + \frac{1}{\hat{R}} + \frac{1}{S_j\hat{L}}\right)\right] + \frac{K^2}{\rho} = 0, \tag{45}$$

whose coefficients and solutions are independent of j. As a consequence, optimizing the poles of Eq. (45) amounts to optimizing the poles corresponding to all the eigenmodes simultaneously, since this optimization supplies optimal values of the parameters $\hat{C}$, $\hat{R}$ and $\hat{L}$ which do not depend on j. The corresponding line admittances $A_0(s)$, $A_2(s)$ and $A_4(s)$ follow from Eq. (28), and turn out to be:

$$\begin{aligned}
&A_0(s) = sC \quad \text{with } C = \varepsilon\hat{C},\\
&A_2(s) = 1/R \quad \text{with } R = \varepsilon\hat{R},\\
&A_4(s) = 1/(sL) \quad \text{with } L = \varepsilon^3\hat{L}.
\end{aligned} \tag{46}$$

7.2. Discrete model

The N_p piezoelectric actuators, up to the first and the last ones, have all the same length $\eta\varepsilon$ and their centers constitute a periodic array of spatial period $\varepsilon = l/(N_p - 1)$. The first and the last actuators have half-length, one end aligned to the support, and are shunted to the ground (see Fig. 1). Accordingly, the remaining actuators will be numbered from 1 to p, where $p = N_p - 2$. Their centers are at the positions εi and are supported on the intervals (z_i^-, z_i^+), where $z_i^\pm = \varepsilon(i \pm \eta/2)$, $i = 1 \dots p$.

The shape functions f_j chosen here are

$$f_j(z) = \sqrt{\frac{2}{\rho l}} \sin(\alpha_j z), \quad j = 1 \dots n, \tag{47}$$

where n is the number of mechanical eigenmodes taken into account in the analysis. Accordingly, it is easily seen that the $n \times n$ mass matrix $\mathbf{M}$ and the $n \times n$ stiffness matrix $\mathbf{K}_{mm}$ in Eq. (10) turns out to be diagonal: in particular, the first one is the identity, while the ith diagonal entry of $\mathbf{K}_{mm}$ is $EJ\alpha_j^4/\rho$. The $n \times p$ matrix $\mathbf{K}_{me}$ is full, and is given by

$$(K_{me})_{ji} = -hb\bar{e}_{31}\alpha_j \sqrt{\frac{2}{\rho l}} \sin(\alpha_j \varepsilon i) \sin\left(\frac{\alpha_j \varepsilon \eta}{2}\right), \quad j = 1 \dots n, \;\; i = 1 \dots p. \tag{48}$$

The $p \times p$ matrix $\mathbf{C}^p$ is diagonal, with diagonal entries all equal to the actuator capacity $C_{ii}^p = \bar{\varepsilon}_{33} b\varepsilon\eta/t$. According to Eq. (17), the $p \times p$ admittance matrix $\mathbf{A}(s)$ is given by

$$\mathbf{A} = A_0\mathbf{M}_0 + A_2\mathbf{M}_2 + A_4\mathbf{M}_4, \tag{49}$$

where the $p \times p$ matrices $\mathbf{M}_0$, $\mathbf{M}_2$ and $\mathbf{M}_4$ are obviously derived from Eq. (17). As an example, in the case $p = 5$ they read as follows:

$$\mathbf{M}_0 = \begin{bmatrix} 1 & 0 & 0 & 0 & 0 \\ 0 & 1 & 0 & 0 & 0 \\ 0 & 0 & 1 & 0 & 0 \\ 0 & 0 & 0 & 1 & 0 \\ 0 & 0 & 0 & 0 & 1 \end{bmatrix}, \quad \mathbf{M}_2 = \begin{bmatrix} 2 & -1 & 0 & 0 & 0 \\ -1 & 2 & -1 & 0 & 0 \\ 0 & -1 & 2 & -1 & 0 \\ 0 & 0 & -1 & 2 & -1 \\ 0 & 0 & 0 & -1 & 2 \end{bmatrix},$$

$$\mathbf{M}_4 = \begin{bmatrix} 5 & -4 & 1 & 0 & 0 \\ -4 & 6 & -4 & 1 & 0 \\ 1 & -4 & 6 & -4 & 1 \\ 0 & 1 & -4 & 6 & -4 \\ 0 & 0 & 1 & -4 & 5 \end{bmatrix}. \tag{50}$$

The admittances connecting the actuators near the simply-supported ends of the beam have been arranged in such a way as to reproduce, at the present discrete level, the boundary conditions $\varphi = 0$ and $-(\hat{A}_4(s)/s)\varphi'' = 0$ given by Eqs. (35) and (36) [15].

Then, the following change of variable is performed

$$\boldsymbol{\varphi} = \mathbf{H}\boldsymbol{\psi}, \tag{51}$$

where the entries of the $p \times p$ matrix $\mathbf{H}$ are given by

$$H_{ij} = \sqrt{\frac{2}{l}}\sin(\alpha_j \varepsilon i), \quad i,j = 1 \ldots p. \tag{52}$$

A similar transformation was adopted in the analysis of rotationally periodic structures (e.g., [13]). Accordingly, the matrices $\mathbf{K}_{me}$, $\mathbf{M}_0$, $\mathbf{M}_2$ and $\mathbf{M}_4$ are transformed into

$$\tilde{\mathbf{K}}_{me} = \mathbf{K}_{me}\mathbf{H}, \quad \tilde{\mathbf{M}}_0 = \mathbf{H}^{\mathrm{T}}\mathbf{H}, \quad \tilde{\mathbf{M}}_2 = \mathbf{H}^{\mathrm{T}}\mathbf{M}_2\mathbf{H}, \quad \tilde{\mathbf{M}}_4 = \mathbf{H}^{\mathrm{T}}\mathbf{M}_4\mathbf{H}. \tag{53}$$

After some computations reported in Appendix A, it is verified that, under the condition

$$p \geqslant n - 1 \tag{54}$$

it turns out that

$$(\tilde{K}_{me})_{ji} = -\frac{K\alpha_j^2}{\sqrt{\rho}} f\left(\frac{\alpha_j \eta \varepsilon}{2}\right)\delta_{ji}, \quad j = 1 \ldots n, \;\; i = 1 \ldots p, \tag{55}$$

$$(\tilde{M}_0)_{ij} = \varepsilon^{-1}\,\delta_{ij}, \quad i,j = 1 \ldots p, \tag{56}$$

$$(\tilde{M}_2)_{ij} = \varepsilon\,\alpha_i^2 g(\alpha_i \varepsilon)\,\delta_{ij}, \quad i,j = 1 \ldots p, \tag{57}$$

$$(\tilde{M}_4)_{ij} = \varepsilon^3\,\alpha_i^4 h(\alpha_i \varepsilon)\,\delta_{ij}, \quad i,j = 1 \ldots p, \tag{58}$$

where δ_{ij} is the Kronecker symbol and

$$f(t) = \frac{\sin t}{t}, \quad g(t) = \frac{2 - 2\cos t}{t^2}, \quad h(t) = \frac{6 - 8\cos t + 2\cos 2t}{t^4}. \tag{59}$$

Accordingly, the governing equations (10) and (11) become uncoupled. In the case $n = p$, they can be written as follows:

$$\begin{bmatrix} \dfrac{EJ}{\rho}\alpha_j^4 + s^2 & -\dfrac{K\alpha_j^2}{\sqrt{\rho}} f\left(\dfrac{\alpha_j \eta \varepsilon}{2}\right) \\ -\dfrac{K\alpha_j^2}{\sqrt{\rho}} f\left(\dfrac{\alpha_j \eta \varepsilon}{2}\right) & -\Gamma - \dfrac{1}{s}[\hat{A}_0(s) + \alpha_j^2 g(\alpha_j \varepsilon)\hat{A}_2(s) + \alpha_j^4 h(\alpha_j \varepsilon)\hat{A}_4(s)] \end{bmatrix} \begin{bmatrix} v_j \\ \psi_j \end{bmatrix} = \begin{bmatrix} \dot{v}_{0j} + s v_{0j} \\ 0 \end{bmatrix} \tag{60}$$

for $j = 1 \ldots n$. Hence, the mechanical unknown v_j, relevant to the mode j, can be controlled due to its coupling with the electrical unknown ψ_j, but each mode is uncoupled from the other ones.

In the case $p > n$, there are $p - n$ electrical equations which do not contain any mechanical unknown and thus they govern the evolution of the electrical parameters ψ_j, $j = n + 1 \ldots p$

independently from any mechanical term. On the other hand, in the case $p \leqslant n-1$, the $(p+1)$th mechanical equation does not contain any electrical unknown, and thus the mechanical unknown v_{p+1} is left uncontrolled. This is because, according to Eq. (48), it results that $(K_{me})_{p+1,i} = 0$, $i = 1 \ldots p$. Moreover, it can be shown that if condition (54) is violated, i.e., if $p < n-1$, the eigenmodes are not uncoupled, since there exist electrical unknowns ψ_j entering more than one mechanical equation. As a consequence, $p = n$ is the minimum value of p which allows

(i) to control all the n mechanical eigenmodes;
(ii) to obtain uncoupled modal equations.

The discrete-model equations (60) differ from the continuous-model ones (38) due to the presence of the multiplicative terms $f(\alpha_j \eta \varepsilon/2)$, $g(\alpha_j \varepsilon)$ and $h(\alpha_j \varepsilon)$, which are, in modulus, strictly less than one. It is interesting to observe that the homogenization limit $\varepsilon \to 0$ can be taken in Eq. (60), supplying Eq. (38), since $f(\alpha_j \eta \varepsilon/2)$, $g(\alpha_j \varepsilon)$ and $h(\alpha_j \varepsilon)$ approach one. It is understood that in this limit the physical admittances $A_0(s)$, $A_2(s)$ and $A_4(s)$ comprising the periodic network are rescaled according to Eq. (28).

8. Optimization of electric networks, simulations and discussion

This section is devoted to the analysis and comparison of the performances of different electric networks. Both periodic and nonperiodic electric networks are considered. Though the latter ones can be applied to any disposition of actuators, they are used here to connect a periodic array of actuators, for the sake of comparison. It is emphasized that nonperiodic networks generally require to tune many electric components at different tuning values; this issue is a difficult task in practical applications, but could be accomplished by including an adaptive fine tuning on the network components [25]. On the other hand, periodic networks have the practical advantage of employing few periodically arranged electric components, thus sensibly reducing tuning problems and manufacturing costs [13]. However, the number of periodically placed actuators they require is lower bounded by the number of eigenmodes to be controlled, as shown in Section 7.2.

The optimization of the periodic networks is performed here according to both the fully continuous model and the fully discrete one, in order to compare the results they supply.

8.1. Case-study structure

A simply supported beam with dimensions $500\,\text{mm} \times 50\,\text{mm} \times 1.5\,\text{mm}$ is considered. It is composed of steel with Young modulus $E = 210\,\text{GPa}$, Poisson ratio $\nu = 0.3$. The linear density ρ of the beam is $0.589\,\text{kg/m}$. The beam is actuated by five piezoelectric PZT actuators, bonded on its surface as shown in Fig. 1, whose dimensions are $66.6 \times 50 \times 0.127\,\text{mm}$. Two halves grounded actuators are added at the beam ends to obtain a periodic actuator arrangement. The reduced clamped permittivity of the actuators in the transversal direction $\bar{\varepsilon}_{33}$ is $10.50\,\text{nF/m}$, and their reduced piezoelectric coupling coefficient $\bar{e}_{31}$ is $17.56\,\text{C/m}^2$. As a consequence, it turns out that $\varepsilon/l = \frac{1}{6}$, $\eta = 0.8$, $\Gamma = 3304\,\text{nF/m}$, and $K = 526.3\,\mu\text{C}$.

8.2. Dimensionless parameters

In this section a dimensionless version of Eqs. (38) and (60) is derived. To this end, the following positions are made:

$$\mathbf{v} = l\,\overline{\mathbf{v}}, \quad \boldsymbol{\varphi} = \frac{l\omega_1}{\sqrt{\Gamma}}\overline{\boldsymbol{\varphi}}, \quad s = \omega_1\overline{s}, \quad K = \overline{K}\sqrt{EJ\Gamma}, \quad \mathbf{v}_0 = l\omega_1\overline{\mathbf{v}}_0, \quad \dot{\mathbf{v}}_0 = l\omega_1^2\overline{\dot{\mathbf{v}}}_0, \tag{61}$$

where the dimensionless counterparts of the involved physical parameters are overlined, and

$$\omega_1 = \left(\frac{\pi}{l}\right)^2\sqrt{\frac{EJ}{\rho}} \tag{62}$$

is the first circular eigenfrequency of the beam at shorted actuators. Of course, the system poles are rescaled as the Laplace variable s, and hence $\mathrm{ETDR} = \omega_1\overline{\mathrm{ETDR}}$.

Accordingly, Eq. (38) is transformed into

$$\begin{bmatrix} j^4+\overline{s}^2 & -j^2\overline{K} \\ -j^2\overline{K} & -1-\dfrac{1}{\omega_1\Gamma\overline{s}}[\hat{A}_0(\omega_1\overline{s})+\alpha_j^2\hat{A}_2(\omega_1\overline{s})+\alpha_j^4\hat{A}_4(\omega_1\overline{s})] \end{bmatrix}\begin{bmatrix} \overline{v}_j \\ \overline{\varphi}_j \end{bmatrix} = \begin{bmatrix} \overline{\dot{v}}_{0j}+\overline{s}\,\overline{v}_{0j} \\ 0 \end{bmatrix} \tag{63}$$

and Eq. (60) is transformed analogously.

By substituting $\hat{A}_0$, $\hat{A}_2$ and $\hat{A}_4$ from Eqs. (44) and (46), Eq. (63) becomes

$$\begin{bmatrix} j^4+\overline{s}^2 & -j^2\overline{K} \\ -j^2\overline{K} & -1-\left(\overline{C}+j^2\dfrac{1}{\overline{s}\overline{R}}+j^4\dfrac{1}{\overline{s}^2\overline{L}}\right) \end{bmatrix}\begin{bmatrix} \overline{v}_j \\ \overline{\varphi}_j \end{bmatrix} = \begin{bmatrix} \overline{\dot{v}}_{0j}+\overline{s}\,\overline{v}_{0j} \\ 0 \end{bmatrix}, \tag{64}$$

where the following positions are made:

$$C = \varepsilon\Gamma\overline{C}, \quad R = \frac{\pi^2\varepsilon}{\omega_1 l^2\Gamma}\overline{R}, \quad L = \frac{\pi^4\varepsilon^3}{\omega_1^2 l^4\Gamma}\overline{L}. \tag{65}$$

The numerical values of the scales of ETDR, K, C, R and L for the structure considered in Section 8.1 are, respectively:

$$\begin{aligned} &\omega_1 = 88.42\ \mathrm{rad/s}, \quad \sqrt{EJ\Gamma} = 3124\,\mu\mathrm{C}, \quad \varepsilon\Gamma = 275.3\,\mathrm{nF}, \\ &\frac{\pi^2\varepsilon}{\omega_1 l^2\Gamma} = 11.26\,\mathrm{k\Omega}, \quad \frac{\pi^4\varepsilon^3}{\omega_1^2 l^4\Gamma} = 34.92\,\mathrm{H}. \end{aligned} \tag{66}$$

Consequently, it turns out that $\overline{K} = 0.1685$.

8.3. Periodic networks

8.3.1. Network configurations

All the periodic networks considered here are derived from the periodic zeroth-, second- and fourth-order lines reported in Figs. 2–4.

The network PNR_2L_2, shown in Fig. 7, was proposed in Ref. [14]. It contains both inductors and resistors on the second-order line. The network PNR_0L_4, shown in Fig. 8, was proposed in Ref. [15]. It contains inductors on a fourth-order line, and resistors on a zeroth-order line. The network PNR_2L_4, shown in Fig. 9 and proposed in Ref. [18], is obtained by modifying the network PNR_0L_4: the resistors R from the zeroth-order line were moved to the second-order line, in order to satisfy the optimal-tuning conditions on all the eigenmodes (44). Consequently, this network is expected to significatively improve over the networks PNR_2L_2 and PNR_0L_4. It is noted that the networks PNR_0L_4 and PNR_2L_4, containing a fourth-order line, employ negative inductances which can be obtained by means of operational amplifiers. The network PNR_0L_4 may

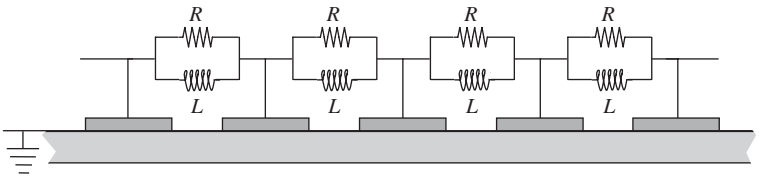

Fig. 7. Periodic electric network PNR_2L_2.

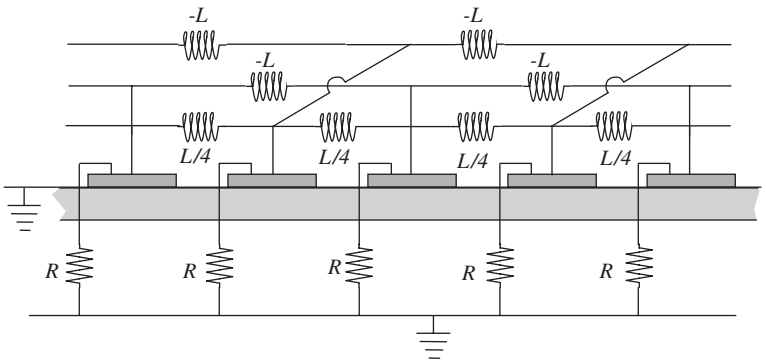

Fig. 8. Periodic electric network PNR_0L_4.

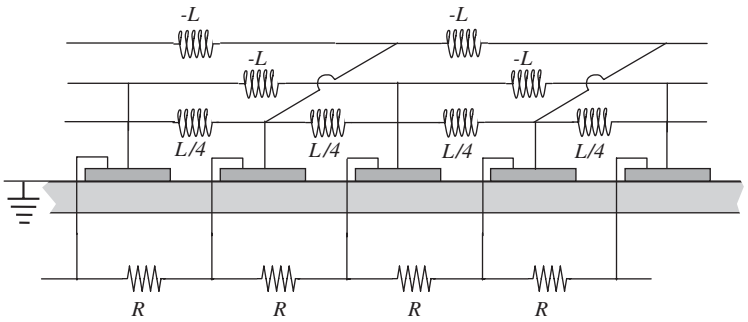

Fig. 9. Periodic electric network PNR_2L_4.

be approximated by a network containing purely passive components [15], which, however, is somewhat complex.

The network PNF_2, shown in Fig. 10, is aimed to be effective on several eigenmodes without employing a fourth-order line. It does not meet the conditions (44). On the other hand, it partially follows Hollkamp's idea [6] to use different parallel *RLC* branches, acting as band-pass filters, connected to a single actuator for damping structural vibrations along different eigenmodes. An effective multimodal damping is achieved here by using only two parallel branches on the second-order line.

Finally, the network PNC_0R_2, shown in Fig. 11, is proposed, containing negative capacitors on the zeroth-order line and resistors on the second-order line. This network meets conditions (44) for optimal tuning on all the eigenmodes. It turns out to be extremely performant; however, it is an active network, since it employs negative capacitors.

The admittance values $A_0(s)$, $A_2(s)$ and $A_4(s)$, entering the continuous-model equation (38) and the discrete-model equation (60) via the scaling (28), are reported in Table 1.

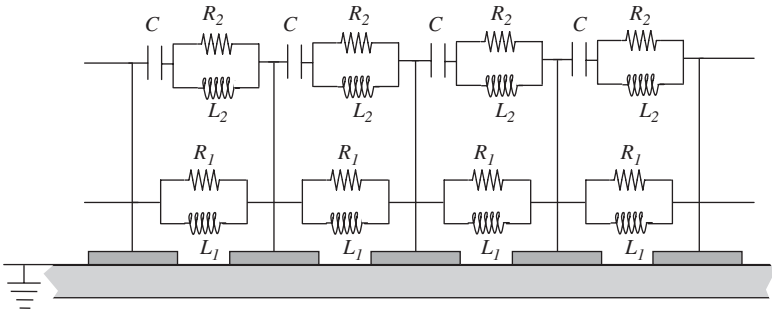

Fig. 10. Periodic electric network PNF_2.

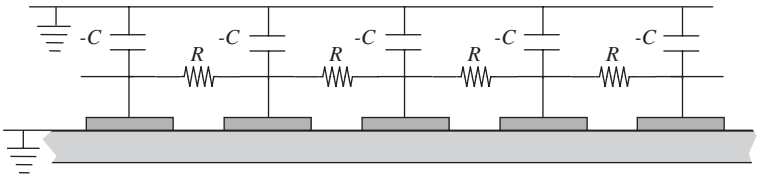

Fig. 11. Periodic electric network PNC_0R_2.

Table 1
Electrical admittances of periodic networks

	PNR_2L_2	PNR_0L_4	PNR_2L_4	PNF_2	PNC_0R_2
$A_0(s)$	0	$1/R$	0	0	$-sC$
$A_2(s)$	$1/R+1/(sL)$	0	$1/R$	F	$1/R$
$A_4(s)$	0	$1/(sL)$	$1/(sL)$	0	0

Here $F = 1/R_1 + 1/(sL_1) + [1/(sC) + sL_2R_2/(R_2 + sL_2)]^{-1}$.

8.3.2. Single-mode optimization according to the continuous model

In this section, the damping of vibrations along a single eigenmode is considered. In particular, an analytical optimization of the networks proposed in Section 8.3.1 is performed on the basis of the continuous model.

The characteristic polynomials of the networks PNR_2L_2, PNR_0L_4 and PNR_2L_4 are fourth-order degree whereas the network PNC_0R_2, which does not contain inductors, has a third-order degree characteristic polynomial. According to the pole placement technique, the optimal damping is achieved when the fourth-order degree polynomials exhibit two coincident couples of complex conjugate roots, whereas the third-order degree polynomials have three coincident real roots [4]. The analytical expressions for the optimal electric components are determined by enforcing these conditions, and are reported, in dimensionless form, in Table 2, together with the corresponding modal exponential time-decay rate $\overline{\lambda}$ and circular frequency $\overline{\omega}$. The network PNF_2 is not considered here, since it contains several parameters leading to complicate analytical expressions. It is remarked that the optimal parameters relevant to the networks PNR_2L_4 and PNC_0R_2 do not depend on the mode number j. In other words, the same optimal choice of the electric parameters optimally performs on all the eigenmodes at the same time, leading to a modal exponential time-decay rate proportional to j^2 (i.e., to the modal eigenfrequency). This is precisely because these two networks satisfy the optimal-tuning conditions (44). This is not the case for the networks PNR_2L_2 and PNR_0L_4, whose optimal parameters depend on j: as a consequence, only a single eigenmode can be optimally damped once the values of R and L have been assigned.

In order to obtain a numerical comparison, the structure presented in Section 8.1 is considered. The numerical values of the electric parameters are chosen in such a way as to optimize the vibration damping along the first eigenmode (i.e., it is taken $j = 1$ in Table 2) and are reported in Table 3. The corresponding values of the modal exponential time-decay rates of the first five

Table 2
Dimensionless electric parameters and modal exponential time-decay rates of periodic networks: single-mode optimization according to the continuous model

	PNR_2L_2	PNR_0L_4	PNR_2L_4	PNC_0R_2
$\overline{C}$	/	/	/	$1-\frac{\overline{K}^2}{8}$
$\overline{R}$	$\frac{1}{2\overline{K}}$	$\frac{1}{2\overline{K}}\frac{1}{(\varepsilon\alpha_j)^2}$	$\frac{1}{2\overline{K}}$	$\frac{8\sqrt{3}}{9}\frac{1}{\overline{K}^2}$
$\overline{L}$	$\frac{1}{(\varepsilon\alpha_j)^2}$	1	1	/
$\overline{\lambda}$	$-j^2\frac{\overline{K}}{2}$	$-j^2\frac{\overline{K}}{2}$	$-j^2\frac{\overline{K}}{2}$	$-j^2\sqrt{3}$
$\overline{\omega}$	$j^2\sqrt{1-\frac{\overline{K}^2}{4}}$	$j^2\sqrt{1-\frac{\overline{K}^2}{4}}$	$j^2\sqrt{1-\frac{\overline{K}^2}{4}}$	0

Table 3
Dimensionless electric parameters of periodic networks: optimization on the first eigenmode according to the continuous model

	PNR_2L_2	PNR_0L_4	PNR_2L_4	PNC_0R_2
$\overline{R}$	2.97	10.82	2.97	54.23
$\overline{L}$	3.65	1	1	/
$\overline{C}$	/	/	/	0.996

Table 4
Dimensionless modal exponential time-decay rates $\overline{\lambda}$ according to the continuous model

Eigenmode	PNR_2L_2	PNR_0L_4	PNR_2L_4	PNC_0R_2
I	−0.084	−0.084	**−0.084**	**−1.73**
II	**−0.027**	**−0.077**	−0.34	−6.93
III	−0.046	**−0.077**	−0.76	−15.59
IV	−0.075	**−0.077**	−1.35	−27.71
V	−0.113	**−0.077**	−2.11	−43.30
$\overline{\text{ETDR}}$	**−0.027**	**−0.077**	**−0.084**	**−1.73**

Electrical parameters chosen as in Table 3.

eigenmodes are reported in Table 4. The lowest value of $\overline{\lambda}$ for each network is given in bold and represents the dimensionless exponential time-decay rate ($\overline{\text{ETDR}}$). These results confirm that the periodic networks which do not satisfy the optimal-tuning conditions (44) exhibit an optimal damping only on the first eigenmode, and a decay in performances on the other eigenmodes. On the other hand, the periodic networks which do satisfy the optimal-tuning conditions exhibit the ideal behavior of $\overline{\lambda}$ proportional to the modal eigenfrequency.

In particular, the network PNC_0R_2 yields a damping definitely higher than the other networks. This is due to the presence of the negative capacitances, able to compensate the inherent capacitance of the piezoelectric actuators, thus reducing the overall reactive electric impedance offered by the piezoelectric actuators. However, this damping must be intended as a theoretical value, since the optimal values of the electric components are quite close to the instability limit [12]: in practical applications, it would be safer to choose electric parameters sufficiently far from that limit, at the cost of reduced performances.

8.3.3. Multimode optimization according to the continuous model

In this section, the multimodal vibration damping is considered. The electric parameters relevant to the networks presented in Section 8.3.1 are chosen such as to optimize the exponential time-decay rate of the free vibrations taking into account the first five structural eigenmodes. The optimization is performed numerically, on the basis of the continuous model equations (38), by means of the Matlab® fminsearch routine. Also the periodic network PNF_2 is here considered, in order to establish its ability in damping multimodal vibrations. The values of the optimized

electric parameters are reported in Table 5 and the corresponding modal exponential time-decay rates are reported in Table 6.

Comparing the entries in Table 6 with the corresponding ones in Table 4, it can be observed that they are coincident for the networks PNR_2L_4 and PNC_0R_2 whereas are different for the networks PNR_2L_2 and PNR_0L_4. Indeed, the former networks satisfy the optimal-tuning conditions (44) and hence optimizing over one eigenmode is equivalent to optimize over all the eigenmodes. On the other hand, the latter imply different optimal electric parameters for different eigenmodes: as a consequence, the numerical optimizer has to achieve a trade-off between the considered eigenmodes, in order to optimize the overall exponential time-decay rates and to improve over the ones obtained in Table 4. In fact, for the network PNR_2L_2 the exponential time-decay rate on the first eigenmode is worsened with respect to the single-mode optimization, whereas the exponential time-decay rate on the second mode is improved to match the rate on the first eigenmode. For the network PNR_0L_4 only a little improvement of the exponential time-decay rate is achieved with respect to the single-mode optimization. Finally, the passive network PNF_2 shows a good ability in damping a multimodal system.

8.3.4. *Multimode optimization according to the discrete model*

As in the previous section, the multimodal vibration damping is considered, but the numerical optimization is here performed according to the discrete model (60). The aim is to evaluate the performances of the electric networks in real situations, where the number of actuators is limited to few units for technological reasons, so that a continuous model may be inaccurate.

Table 5
Dimensionless electric parameters of periodic networks: optimization on the first five eigenmodes according to the continuous model

	PNR_2L_2	PNR_0L_4	PNR_2L_4	PNC_0R_2	PNF_2
$\overline{R}$	2.12	10.83	2.97	54.23	2.75, 21.26
$\overline{L}$	3.44	1.00	1	/	3.17, 2.63
$\overline{C}$	/	/	/	0.996	0.495

In the last column the first (respectively, second) entries refer to $\overline{R}_1$, $\overline{L}_1$ (respectively, $\overline{R}_2$, $\overline{L}_2$).

Table 6
Dimensionless modal exponential time-decay rates $\overline{\lambda}$ according to the continuous model

Eigenmode	PNR_2L_2	PNR_0L_4	PNR_2L_4	PNC_0R_2	PNF_2
I	**−0.034**	**−0.078**	**−0.084**	**−1.73**	**−0.078**
II	**−0.034**	**−0.078**	−0.34	−6.93	**−0.078**
III	−0.059	**−0.078**	−0.76	−15.59	**−0.078**
IV	−0.096	**−0.078**	−1.35	−27.71	−0.10
V	−0.14	**−0.078**	−2.11	−43.30	−0.15
$\overline{\text{ETDR}}$	**−0.034**	**−0.078**	**−0.084**	**−1.73**	**−0.078**

Electrical parameters chosen as in Table 5.

The discrete model supplies values for the electric components (Table 7) and the modal exponential time-decay rates (Table 8) which are different from the corresponding quantities obtained by using the continuous model, given in Section 8.3.3.

It is pointed out that the discrete-model equations (60) may be taken formally to coincide with the continuous-model equations (38), if the homogenized structural piezoelectric coupling coefficient K is replaced by $f(\alpha_j\eta\varepsilon/2)K$, and the second- and fourth-order admittances $A_2(s)$ and $A_4(s)$ are, respectively, replaced by $g(\alpha_j\varepsilon)A_2(s)$ and $h(\alpha_j\varepsilon)A_4(s)$. The coefficients $f(\alpha_j\eta\varepsilon/2)$, $g(\alpha_j\varepsilon)$ and $h(\alpha_j\varepsilon)$, reported in Table 9, do depend on the mode number j: as a consequence, the optimal-tuning conditions (44) for the continuous model do not hold when the discrete model is adopted.

Table 7
Dimensionless electric parameters of periodic networks: optimization on the first five eigenmodes according to the discrete model

	PNR_2L_2	PNR_0L_4	PNR_2L_4	PNC_0R_2	PNF_2
$\overline{R}$	1.96	4.73	2.92	53.79	2.54, 7.82
$\overline{L}$	3.35	0.80	0.96	/	2.74, 1.79
$\overline{C}$	/	/	/	0.997	0.972

In the last column the first (respectively, second) entries refer to $\overline{R}_1$, $\overline{L}_1$ (respectively, $\overline{R}_2$, $\overline{L}_2$).

Table 8
Dimensionless modal exponential time-decay rates $\overline{\lambda}$ according to the discrete model

Eigenmode	PNR_2L_2	PNR_0L_4	PNR_2L_4	PNC_0R_2	PNF_2
I	**−0.031**	**−0.018**	**−0.084**	**−1.73**	**−0.072**
II	**−0.031**	−0.15	−0.15	−4.09	−0.073
III	−0.046	−0.11	−0.15	−7.41	**−0.072**
IV	−0.059	−0.040	−0.12	−10.78	−0.073
V	−0.064	**−0.018**	**−0.084**	−13.74	**−0.072**
$\overline{\text{ETDR}}$	**−0.031**	**−0.018**	**−0.084**	**−1.73**	**−0.072**

Electrical parameters chosen as in Table 7.

Table 9
Coefficients $f(\alpha_j\eta\varepsilon/2)$, $g(\alpha_j\varepsilon)$ and $h(\alpha_j\varepsilon)$, for the eigenmodes $j = 1 \ldots 5$

Eigenmode	$f(\alpha_j\eta\varepsilon/2)$	$g(\alpha_j\varepsilon)$	$h(\alpha_j\varepsilon)$
I	0.9927	0.9774	0.9552
II	0.9711	0.9119	0.8315
III	0.9356	0.8106	0.6570
IV	0.8873	0.6839	0.4677
V	0.8273	0.5445	0.2965

However, these conditions turn out to be an excellent design tool: indeed, the electric networks PNR_2L_4 and PNC_0R_2, designed according to Eq. (44), exhibit in Table 8 almost the same exponential time-decay rates shown in Table 6, at the cost of consuming the great amount of damping on higher-frequency modes predicted by the continuous model.

On the other hand, the networks PNR_0L_4 and PNR_2L_2, which do not satisfy the optimal-tuning conditions, exhibit in Table 8 smaller exponential time-decay rates than the ones in Table 6. The decrease in performances is more significant for PNR_0L_4 than for PNR_2L_2. As a matter of fact, both of them are mistuned on higher frequencies: the latter because the optimal value of the inductance is proportional to j^2 (see Table 2); the former due to the coefficient $h(\alpha_j\varepsilon)$ which appear in the discrete model: indeed, even a little mistuning severely worsen the performance [4]. Hence, the modal exponential time-decay rates on higher frequencies for both these networks depend only on the value of the resistance, which is not far from the correct one (up to $g(\alpha_j\varepsilon)$, being of the order of one) for PNR_2L_2, and is completely incorrect for PNR_0L_4 because the optimal value of the resistance is proportional to j^2 (see Table 2).

Finally, the network PNF_2 exhibits a remarkable exponential time-decay rate even when the discrete model is adopted (Table 8). It is emphasized that such a performance is obtained by using only standard passive components. The two parallel branches behave like electric filters, enabling a proper damping on low- and high-frequency eigenmodes, respectively. Hence, the network PNF_2 is a very good compromise between simplicity in implementation and effectiveness in multimodal damping.

As a concluding remark, it can be observed that the difference between the results supplied by the continuous model (Tables 5 and 6) and the ones supplied by the discrete model (Tables 7 and 8) is not negligible. Hence, though the former is suitable for preliminary design purposes, the use of the latter is mandatory for final implementations.

The present comparison was performed in the case of a simply-supported beam, which allowed closed-form computations according to both the continuous and the discrete model. However, the numerical computations in Ref. [18] showed that the same order of merit of the considered networks prevails for different boundary conditions.

8.4. Nonperiodic networks

Beam vibration control by means of nonperiodic networks is here investigated.

The simplest nonperiodic network considered is the network $NPNR_0L_0$, shown in Fig. 12. It is composed by standard *RL*-parallel shunt circuits, each one connected to a piezoelectric actuator.

The network $NPNR_2L_2$, shown in Fig. 13, is obtained by connecting each piezoelectric actuator to the adjacent ones by means of a *RL*-parallel shunt circuit.

In order to evaluate the performances of those nonperiodic networks, a numerical optimization is performed on the basis of the discrete model reported in Section 3. The shape functions $f_j(z)$ appearing in Eq. (9) are chosen as in Eq. (47).

It is emphasized that Eqs. (12) and (13) cannot be decoupled into independent equations for each eigenmode, due to the nonperiodic character of the networks. Moreover, the number of parameters to be optimized in the present case is in general higher than in the case of periodic networks, leading to a difficult numerical optimization problem.

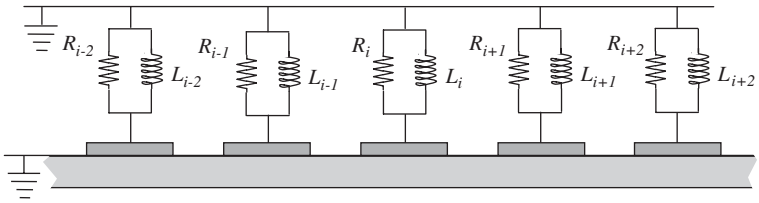

Fig. 12. Nonperiodic electric network $NPNR_0L_0$.

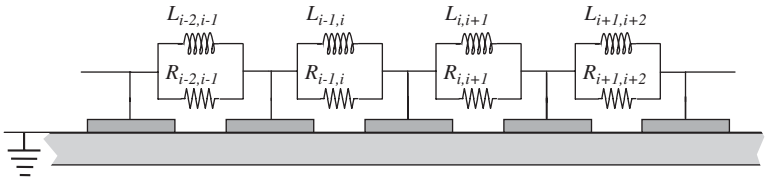

Fig. 13. Nonperiodic electric network $NPNR_2L_2$.

Table 10
Dimensionless optimal electric parameters for the nonperiodic networks $NPNR_0L_0$ and $NPNR_2L_2$

$NPNR_0L_0$		$NPNR_2L_2$	
$\overline{R}_1 = 9.35$	$\overline{L}_1 = 0.822$	$\overline{R}_{0,1} = 4.27$	$\overline{L}_{0,1} = 5.16$
$\overline{R}_2 = 15.17$	$\overline{L}_2 = 12.50$	$\overline{R}_{1,2} = 0.509$	$\overline{L}_{1,2} = 0.984$
$\overline{R}_3 = 15.66$	$\overline{L}_3 = 13.69$	$\overline{R}_{2,3} = 30.70$	$\overline{L}_{2,3} = 0.584$
$\overline{R}_4 = 0.434$	$\overline{L}_4 = 0.0355$	$\overline{R}_{3,4} = 1.67$	$\overline{L}_{3,4} = 0.470$
$\overline{R}_5 = 0.779$	$\overline{L}_5 = 0.151$	$\overline{R}_{4,5} = 1.11$	$\overline{L}_{4,5} = 7.43$
		$\overline{R}_{5,6} = 86.67$	$\overline{L}_{5,6} = 4.26$

The optimal electric parameters are reported in Table 10. In order to evaluate the exponential time-decay rate, all the complex poles of system (12) and (13) are evaluated and reported in Table 11 in dimensionless form: the real part of the poles correspond to the dimensionless modal exponential time-decay rate $\overline{\lambda}$, whereas the imaginary part $\overline{\omega}$ is the corresponding dimensionless circular frequency. It can be observed that both the networks $NPNR_0L_0$ and $NPNR_2L_2$ are able to furnish an effective multimodal damping, which is close to the damping supplied by the PNR_2L_4 network. However, the nonperiodic networks require to tune many electric parameters at different tuning values.

9. Conclusion

The optimal design of electric networks for vibration damping of a piezoactuated beam was studied. Both a continuous-homogenized model and a discrete model were proposed for the dynamical analysis of the controlled structure. The former supplied a simple analytical condition

Table 11
Dimensionless pole couples relevant to the nonperiodic networks $NPNR_0L_0$ and $NPNR_2L_2$

Pole couples	$NPNR_0L_0$		$NPNR_2L_2$	
I	**−0.078**	± 0.99 *I*	**−0.087**	± 1.00 *I*
II	**−0.078**	± 1.00 *I*	**−0.087**	± 1.00 *I*
III	**−0.078**	± 1.00 *I*	−0.77	± 3.66 *I*
IV	−0.10	± 3.87 *I*	−0.13	± 4.08 *I*
V	−0.091	± 4.13 *I*	−2.14	± 7.70 *I*
VI	**−0.078**	± 9.07 *I*	−0.089	± 9.14 *I*
VII	−2.24	± 9.08 *I*	−0.091	± 16.13 *I*
VIII	**−0.078**	± 16.11 *I*	**−0.087**	± 25.23 *I*
IX	−4.08	± 18.90 *I*	−1.41, −3.09	+ 0 *I*
X	**−0.078**	± 25.27 *I*	−3.51, −11.44	+ 0 *I*
$\overline{\text{ETDR}}$	**−0.078**		**−0.087**	

for the optimal design of periodic networks. The latter turned out to be a necessary tool for evaluating the performances of designed networks in practical applications. The new proposed networks exhibited good performances in multimodal damping and improved over existing ones.

Acknowledgements

The authors wish to thank the anonymous referees for their valuable comments on this paper. The financial supports of CNR and MIUR are gratefully acknowledged. This research was developed within the framework of Lagrange Laboratory, an European research group between CNRS, CNR, University of Rome "Tor Vergata", University of Montpellier II, ENPC and LCPC.

Appendix A. Discrete model for the simply-supported beam: change of variable

This appendix is aimed to derive Eqs. (55)–(58), yielding the transformed matrices $\tilde{\mathbf{K}}_{me}$, $\tilde{\mathbf{M}}_0$, $\tilde{\mathbf{M}}_2$ and $\tilde{\mathbf{M}}_4$ obtained from Eq. (53) after the change of variable (51).

A.1. Preliminaries

The following well-known identities will be instrumental in the computations:

$$\sum_{j=0}^{N} \cos jz = \begin{cases} N+1 & \text{if } z \equiv 0 \bmod 2\pi \\ \cos\dfrac{Nz}{2}\dfrac{\sin[((N+1)z)/2]}{\sin(z/2)} & \text{otherwise} \end{cases} \tag{A.1}$$

and

$$\sum_{j=0}^{N} \sin jz = \begin{cases} 0 & \text{if } z \equiv 0 \bmod 2\pi \\ \sin\dfrac{Nz}{2}\dfrac{\sin[((N+1)z)/2]}{\sin(z/2)} & \text{otherwise,} \end{cases} \tag{A.2}$$

where $N \in \mathbf{N}$, $z \in \mathbf{R}$ and $\equiv$ means congruent. The proof of Eqs. (A.1) and (A.2) is easily obtained by noting that their left-hand sides are, respectively, the real part and the coefficient of the imaginary part of the geometric series $\sum_{j=0}^{N} u^j$, where $u = \exp(\mathrm{I}z)$.

The above identities are then specialized to the case when $N = p + 1$ and $z = m\pi/(p + 1)$, with $m \in \mathbf{Z}$, leading to the identities:

$$\sum_{j=0}^{p+1} \cos\frac{jm\pi}{p+1} = \begin{cases} p+2 & \text{if } m \equiv 0 \bmod 2(p+1), \\ 1 & \text{if } m \text{ is even, and } m \not\equiv 0 \bmod 2(p+1), \\ 0 & \text{if } m \text{ is odd} \end{cases} \tag{A.3}$$

and

$$\sum_{j=0}^{p+1} \sin\frac{jm\pi}{p+1} = \begin{cases} 0 & \text{if } m \text{ is even,} \\ \cot\dfrac{m\pi}{2(p+1)} & \text{if } m \text{ is odd.} \end{cases} \tag{A.4}$$

If the sum at the left-hand side of Eq. (A.4) is carried out for j from 1 to p, the result is unchanged; on the other hand, Eq. (A.3) is transformed into:

$$\sum_{j=1}^{p} \cos\frac{jm\pi}{p+1} = \begin{cases} p & \text{if } m \equiv 0 \bmod 2(p+1), \\ -1 & \text{if } m \text{ is even, and } m \not\equiv 0 \bmod 2(p+1), \\ 0 & \text{if } m \text{ is odd.} \end{cases} \tag{A.5}$$

A.2. The transformed matrix $\tilde{\mathbf{K}}_{me}$

In this section, Eq. (55) is proved. It turns out that

$$(\tilde{K}_{me})_{ji} = \sum_{q=1}^{p} (K_{me})_{jq} H_{qi} = -\frac{hb\bar{e}_{31}\alpha_j}{l\sqrt{\rho}} \sin\left(\frac{\alpha_j \varepsilon \eta}{2}\right) \sum_{q=1}^{p} 2\,\sin(\alpha_j \varepsilon q)\sin(\alpha_i \varepsilon q). \tag{A.6}$$

By using Eq. (A.5) and remembering that $1 \leqslant j \leqslant n$ and $1 \leqslant i \leqslant p$, it follows that

$$\sum_{q=1}^{p} 2\,\sin(\alpha_j \varepsilon q)\sin(\alpha_i \varepsilon q) = \sum_{q=1}^{p} \cos\frac{q(j-i)\pi}{p+1} - \sum_{q=1}^{p} \cos\frac{q(j+i)\pi}{p+1} = (p+1)\delta_{ji}. \tag{A.7}$$

Indeed, if $j \neq i$, the quantities $j - i$ and $j + i$ have the same evenness, and are not congruent to zero modulo $2(p + 1)$, as a consequence of condition (54), so that the sums on the second term of the previous equation are equal; if $j = i$, reasoning as above, one finds that the first sum is equal to p, whereas the second one is equal to -1. Eq. (55) readily follows from Eqs. (A.6) and (A.7).

A.3. The transformed matrix $\tilde{\mathbf{M}}_0$

In this section, Eq. (56) is proved. Let $\mathbf{w}^{(j)}$ be the jth column of the matrix $\mathbf{H}$:

$$w_i^{(j)} = H_{ij} = \sqrt{\frac{2}{l}}\sin(\alpha_j \varepsilon i). \tag{A.8}$$

Reasoning as in Section A.2, it turns out that

$$\begin{aligned}(\tilde{M}_0)_{ij} = \mathbf{w}^{(i)} \cdot \mathbf{w}^{(j)} &= \sum_{q=1}^{p} w_q^{(i)} w_q^{(j)} = \frac{1}{l}\sum_{q=1}^{p} 2\,\sin(\alpha_i \varepsilon q)\sin(\alpha_j \varepsilon q) \\ &= \frac{p+1}{l}\delta_{ij} = \frac{1}{\varepsilon}\delta_{ij}.\end{aligned} \tag{A.9}$$

Hence, in particular, the vectors $\mathbf{w}^{(j)}$, $j = 1 \ldots p$, constitute an orthogonal basis of $\mathbf{R}^p$.

A.4. The transformed matrix $\tilde{\mathbf{M}}_2$

In this section, Eq. (57) is proved. According to Eq. (A.9), it is sufficient to prove that $\mathbf{w}^{(j)}$ is an eigenvector of the matrix $\mathbf{M}_2$, and the corresponding eigenvalue is $(\alpha_j \varepsilon)^2 g(\alpha_j \varepsilon)$. Indeed, setting $\mathbf{z}^{(j)} = \mathbf{M}_2 \mathbf{w}^{(j)}$, it turns out that

$$\begin{aligned} z_i^{(j)} &= -w_{i-1}^{(j)} + 2w_i^{(j)} - w_{i+1}^{(j)} \\ &= \sqrt{\frac{2}{l}}[-\sin(i-1)\alpha_j \varepsilon + 2\,\sin i\alpha_j \varepsilon - \sin(i+1)\alpha_j \varepsilon] = 2(1-\cos\alpha_j \varepsilon)\sqrt{\frac{2}{l}}\sin i\alpha_j \varepsilon \\ &= 2(1-\cos\alpha_j \varepsilon)\, w_i^{(j)} = (\alpha_j \varepsilon)^2 g(\alpha_j \varepsilon)\, w_i^{(j)}. \end{aligned} \tag{A.10}$$

The previous equation holds for $2 \leqslant i \leqslant p-1$, but the same computation applies to the cases $i = 1$ and $i = p$, by setting $w_0^{(j)} = w_{p+1}^{(j)} = 0$, in agreement with Eq. (A.8).

A.5. The transformed matrix $\tilde{\mathbf{M}}_4$

In this section Eq. (58) is proved. As in the previous case, it is sufficient to prove that $\mathbf{w}^{(j)}$ is an eigenvector of the matrix $\mathbf{M}_4$, and the corresponding eigenvalue is $(\alpha_i \varepsilon)^4 h(\alpha_i \varepsilon)$. Indeed, setting $\mathbf{z}^{(j)} = \mathbf{M}_4 \mathbf{w}^{(j)}$, it turns out that

$$\begin{aligned} z_i^{(j)} &= w_{i-2}^{(j)} - 4w_{i-1}^{(j)} + 6w_i^{(j)} - 4w_{i+1}^{(j)} + w_{i+2}^{(j)} \\ &= \sqrt{\frac{2}{l}}[\sin(i-2)\alpha_j \varepsilon - 4\sin(i-1)\alpha_j \varepsilon + 6\sin i\alpha_j \varepsilon - 4\sin(i+1)\alpha_j \varepsilon + \sin(i+2)\alpha_j \varepsilon] \\ &= 2(3 - 4\cos\alpha_j \varepsilon + \cos 2\alpha_j \varepsilon)\sqrt{\frac{2}{l}}\sin i\alpha_j \varepsilon \\ &= 2(3 - 4\cos\alpha_j \varepsilon + \cos 2\alpha_j \varepsilon)\, w_i^{(j)} = (\alpha_j \varepsilon)^4 h(\alpha_j \varepsilon)\, w_i^{(j)}. \end{aligned} \tag{A.11}$$

The previous equation holds for $3 \leqslant i \leqslant p-2$, but the same computation applies to the cases $i = 1, 2$ and $i = p-1, p$, by setting $w_0^{(j)} = w_{p+1}^{(j)} = 0$, $w_{-1}^{(j)} = -w_1^{(j)}$ and $w_{p+2}^{(j)} = -w_p^{(j)}$, in agreement with Eq. (A.8).

References

[1] D.J. Inman, Vibration suppression through smart damping, in: *Proceedings of the 5th International Congress on Sound and Vibration*, Adelaide, South Australia, 1997.

[2] E.F. Crawley, J. de Luis, Use of piezoelectric actuators as elements of intelligent structures, *AIAA Journal* 25 (1987) 1373–1385.

[3] P. Bisegna, G. Caruso, D. Del Vescovo, S. Galeani, L. Menini, Semi-active control of a thin piezoactuated structure, in: T.T. Hyde (Ed.), *Smart Structures and Materials 2000: Damping and Isolation*, *SPIE Proceedings*, vol. 3989, SPIE, 2000, pp. 301–311.

[4] N.W. Hagood, A. von Flotow, Damping of structural vibrations with piezoelectric materials and passive electrical network, *Journal of Sound and Vibration* 146 (2) (1991) 243–268.

[5] G. Caruso, A critical analysis of electric shunt circuits employed in piezoelectric passive vibration damping, *Smart Materials and Structures* 10 (5) (2001) 1059–1068.

[6] J.J. Hollkamp, Multimodal passive vibration suppression with piezoelectric materials and resonant shunts, *Journal of Intelligent Material Systems and Structures* 5 (1994) 49–56.

[7] A.J. Fleming, S. Behrens, S.O.R. Moheimani, Reducing the inductance requirements of piezoelectric shunt damping systems, *Smart Materials and Structures* 12 (2003) 57–64.

[8] S.Y. Wu, Method for multiple mode shunt damping of structural vibration using a PZT transducer, in: L. Porter Davis (Ed.), *Smart Structures and Materials 1998*: *Damping and Isolation*, *SPIE Proceedings*, vol. 3327, SPIE, 1998, pp. 159–168.

[9] R.L. Forward, Electromechanical transducer-coupled mechanical structure with negative capacitance compensation circuit, U.S. Patent #04158787, 1979.

[10] J. Tang, K.W. Wang, Active-passive hybrid piezoelectric networks for vibration control: comparisons and improvement, *Smart Materials and Structures* 10 (2001) 794–806.

[11] S. Behrens, A.J. Fleming, S.O.R. Moheimani, A broadband controller for shunt piezoelectric damping of structural vibration, *Smart Materials and Structures* 12 (2003) 18–28.

[12] P. Bisegna, G. Caruso, Structural vibration damping by using piezoelectric actuators and negative capacitances, in: *Proceedings of the XXXII AIAS National Conference*, Salerno, Italy, 2003.

[13] J. Tang, K.W. Wang, Vibration control of rotationally periodic structures using passive piezoelectric shunt networks and active compensation, *Journal of Vibration and Acoustics* 121 (1999) 379–390.

[14] S. Vidoli, F. dell'Isola, Modal coupling in one-dimensional electro-mechanical structured continua, *Acta Mechanica* 141 (2000) 37–50.

[15] S. Alessandroni, F. dell'Isola, M. Porfiri, A revival of electric analogs for vibrating mechanical systems aimed to their efficient control by pzt actuators, *International Journal of Solids and Structures* 39 (2002) 5295–5324.

[16] J. Tang, K.W. Wang, Vibration delocalization of nearly periodic structures using coupled piezoelectric networks, *Journal of Vibration and Acoustics* 125 (2003) 95–108.

[17] O. Thorp, M. Ruzzene, A. Baz, Attenuation and localization of wave propagation in rods with periodic shunted piezoelectric patches, *Smart Materials and Structures* 10 (2001) 979–989.

[18] P. Bisegna, G. Caruso, F. Maceri, Vibration damping by piezoelectric actuators and electrical networks, in: C. Alessandri (Ed.), *CD Proceedings of the XVI AIMETA National Conference*, Ferrara, Italy, 2003.

[19] T. Ikeda, *Fundamentals of Piezoelectricity*, Oxford University Press, Oxford, 1990.

[20] P. Bisegna, A theory of piezoelectric laminates, *Atti della Accademia Nazionale dei Lincei. Classe di Scienze Fisiche, Matematiche e Naturali. Rendiconti Lincei. Serie IX. Matematica e Applicazioni* 8 (1997) 137–165.

[21] P. Bisegna, G. Caruso, Mindlin-type finite elements for piezoelectric sandwich plates, *Journal of Intelligent Material Systems and Structures* 11 (2000) 14–25.

[22] P. Bisegna, G. Caruso, Evaluation of higer-order theories of piezoelectric plates in bending and in stretching, *International Journal of Solids and Structures* 38 (2001) 8805–8830.
[23] J.-L. Lions, E. Magenes, *Non-Homogeneous Boundary Value Problems and Applications*, Springer, New York, 1972.
[24] N.D. Botkin, Homogenization of an equation describing linear thin plates excited by piezopatches, *Communications in Applied Analysis* 3 (1999) 271–281.
[25] D. Niederberger, A. Fleming, S.O.R. Moheimani, M. Morari, Adaptive multi-mode resonant piezoelectric shunt damping, *Smart Materials and Structures* 13 (2004) 1025–1035.